Journal of Innovative Optical Health Sciences
Vol. 11, No. 4 (2018) 1850019 (19 pages)

DOI: 10.1142/S1793545818500190

In vivo percutaneous reflectance spectroscopy of fatty liver development in rats suggests that the elevation of the scattering power is an early indicator of hepatic steatosis

Daqing Piao[*,†,¶], Jerry W. Ritchey[‡], G. Reed Holyoak[†], Corey R. Wall[†], Nigar Sultana[§,‖], Jill K. Murray[†] and Kenneth E. Bartels[†]

[*]*School of Electrical and Computer Engineering*
Oklahoma State University, 202 Engineering South
Stillwater, OK 74078, USA

[†]*Department of Veterinary Clinical Sciences*
Center for Veterinary Health Sciences
002 VTH, Oklahoma State University
Stillwater, OK 74078, USA

[‡]*Department of Veterinary Pathobiology*
Center for Veterinary Health Sciences
Oklahoma State University, 250 McElroy Hall
Stillwater, OK 74078, USA

[§]*Graduate Program on Interdisciplinary Sciences*
Oklahoma State University, Stillwater, OK 74078, USA
[¶]*daqing.piao@okstate.edu*

Received 2 September 2017
Accepted 15 April 2018
Published 11 May 2018

This study assessed whether there was a scattering spectral marker quantifiable by reflectance measurements that could indicate early development of hepatic steatosis in rats for potential applications to pre-procurement organ evaluation. Sixteen rats were fed a methionine-choline-deficient (MCD) diet and eight rats were fed a normal diet. Direct assessment of the liver parenchyma of rats *in vivo* was performed by percutaneous reflectance spectroscopy using a single fiber probe at the beginning of diet-intake and arbitrary post-diet-intake times up to 11 weeks to render longitudinal comparison. Histological sampling of the liver over the duration of diet administration was performed on two MCD-diet treated rats and one control rat euthanized after reflectance spectroscopy measurement. The images of hematoxylin/eosin-stained

[¶]Corresponding author.
[‖]Current address: P3 Group, Southfield, MI 48034, USA

liver specimens were analyzed morphometrically to evaluate the lipid size changes associated with the level of steatosis. The MCD-diet-treated group ($n = 16$) had mild steatosis in seven rats, moderate in three rats, severe in six rats, and no other significant pathology. No control rats ($n = 8$) developed hepatic steatosis. Among the parameters retrieved from per-SfS, only the scattering power (can be either positive or negative) appeared to be statistically different between MCD-treated and control livers. The scattering power for the 16 MCD-diet-treated livers at the time of euthanasia and presenting various levels of steatosis was 0.33 ± 0.21, in comparison to 0.036 ± 0.25 of the eight control livers ($p = 0.0189$). When evaluated at days 12 and 13 combined, the scattering power of the 16 MCD-diet-treated livers was 0.32 ± 0.17, in comparison to 0.10 ± 0.11 of the eight control livers ($p = 0.0017$). All of four MCD-treated livers harvested at days 12 and 13 presented mild steatosis with sub-micron size lipid droplets, even though none of the MCD-treated livers were sonographically remarkable for fatty changes. The elevation of the scattering power may be a valuable marker indicating early hepatic steatosis before the steatosis is sonographically detectable.

Keywords: Hepatic steatosis; diffuse reflectance spectroscopy; liver transplant.

1. Introduction

Fatty livers are used to address the severe donor organ shortage in liver transplantation[1] in the United States[2] and worldwide. Livers with mild level of steatosis, preferrably morphometrically microvesicular type of steatosis,[3] are considered for transplant. Microvesicular steatosis is not associated with primary graft nonfunction after transplantation.[4] In contrast, macrovesicular steatosis is a known risk factor to ischmetic reperfusion injury[5,6] post transplantation and could cause adverse outcomes in living donors who undergo right hepatectomy.[7] There is curently a rising challenge for robust, rapid, and accurate assessment of fatty liver in both deceased and living donors for liver transplant.[3–7]

Histopathological evaluation of liver biopsy specimens grades steatosis according to a semi-quantitative metrics[8]: a grade of "absent" for $<5\%$ hepatocytes affected by lipid infiltration, "mild" for 5% to $<30\%$ infiltration, "moderate" for 30% to $<60\%$ infiltration, and "severe" for $\geq 60\%$ infiltration. Gross assessment of the liver by visual inspection and palpation has shown low accuracy of identifying the parenchyma steatosis.[9,10] Imaging modalities such as computed tomography and magnetic resonance imaging/spectroscopy provide highly accurate assessment of hepatic steatosis[11] but may be logistically unfit for procurements. Ultrasound (US) imaging is the *de facto* modalidy for bedside evaluation of steatosis using specific diagnostic markers including hepato-renal index.[12] Ultrasound imaging, however, lacks the sensitivity to reliably identify livers with mild level of steatosis.[13] Alternative imaging or sensing tools have been investigated for potentially bedside real-time quantification of fatty content in liver tissue.[14] Xu *et al.*[15] demonstrated photoacoustic spectrum analysis for differentiating fatty from normal livers. Other optical spectroscopic methods were applied in various forms and clinical operatabilities. Evers *et al.*[16] and Westerkamp *et al.*[17] used needle-based diffuse reflectance spectroscopy (DRS) over a broad visible-near-infrared spectrum up to 1600 nm for measuring within the liver parenchyma. It was shown that the strong lipid absorption around 1210 nm was a robust diagnostic marker for identifying hepatic steatosis in human liver specimen or during the surgery.[16] Nilsson *et al.*[18] reported that surface DRS measurements from normal or tumorous liver represented the whole liver. A time-resolved near-infrared spectroscopy study by Kitai *et al.*[19] on rat liver specimens with different levels of diet-induced fatty changes revealed that fatty liver presented lower absorption coefficient (μ_a) and higher reduced scattering coefficient (μ_s') when compared with normal liver, suggesting the fat droplets inside the hepatocytes as the dominant scatterers over the visible to near-infrared spectrum. However, the robustness of detecting lipid deposition using the absorption of lipid that is prominent at 1210 nm degrades as the amount of lipid reduces, making it less sensitive or less specific for detecting mild level of steatosis.[16,18]

There was also interest in whether the scattering information alone acquired over a spectral range not

sensitive to lipid absorption could signify the onset of steatosis. Surface measurements on human liver specimens by McLaughlin *et al.*[20] using DRS over 550–1040 nm showed a correlation between the diffuse reflectance intensity and the histological lipid mass fraction of liver tissue. DRS has also shown to complement liver biopsy for grading hepatic fibrosis in paraffin-preserved human liver specimens.[21] While the increased lipid content is expected to globally increase the diffuse reflectance of a fatty liver in comparison to a lean liver,[20] the onset of lipid droplets and the changes of the lipid droplet size shall also alter the spectral dependence of the scattering. Evers *et al.*[16] have already hypothesized that lipid infiltration changes the scattering power — the indicator of the scattering spectral dependence. This hypothesis, however, remained unexamined until now.

This study reports that the fatty changes of livers could cause the elevation of the scattering power, at the early stage of hepatic steatosis development even when the steatosis was unremarkable on ultrasonography. There is currently no alternative way to estimate the scattering power of a bulk tissue *in vivo* other than isolating the contribution of it to the scattering spectrum acquired by reflectance spectroscopy.[22] This study thus employed a minimally invasive approach of percutaneous single-fiber spectroscopy (per-SfS) to allow direct sampling of the liver parenchyma during longitudinal evaluation of the same liver undergoing steatosis development. This study also used the histopathological imagery to analyze how the size of lipid droplets changed at different levels of steatosis. The changes of the lipid size at the early stage of the steatosis provided morphometric evidence of the changes of the scattering power resolved from the per-SfS measurements.

2. Methods and Materials

2.1. *Animals — Diets and timelines*

The animal study was approved by the Institutional Animal Care and Use Committee of Oklahoma State University (protocol #VM-11-20). A total of 24 rats were separated into two phases (referred to as phase-I and phase-II, as shown in Fig. 1) a few months apart, each having 12 animals and lasting up to a total of 12 weeks including the initial period of acclimation. The separation of the study to two phases was necessary due to scheduling difficulties in overlapping the research times of J. W. R., G. R. H. who rotated with C. R. W., and K. E. B. During each of the two phases, 12 male Sprague-Dawley rats weighing 250–280 g (Harlan Labs, Inc., Madison, WI, USA) were housed individually in the University's Lab Animal Resources facility. All rats

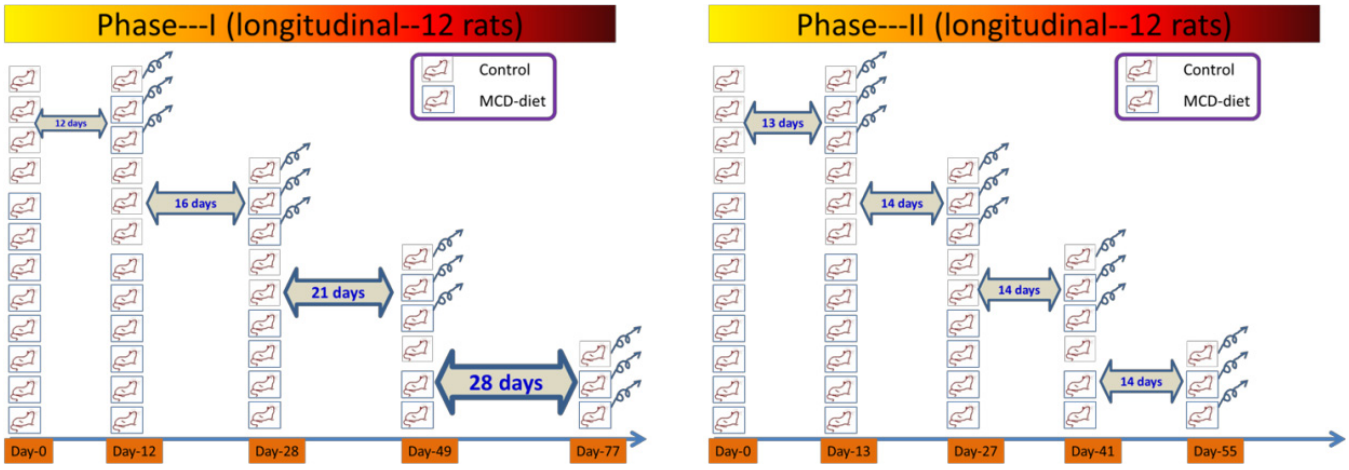

Fig. 1. The timelines of the two phases of the animal study. (a) In phase-I, the histopathology results of the livers were obtained from one control rat and two MCD-diet-treated rats after the *in vivo* per-SfS measurements, on day 12, day 28, day 49, and day 77, respectively. (b) In phase-II, histopathology results of the livers were obtained from one control rat and two MCD-diet-treated rats after the *in vivo* per-SfS measurements, on day 13, day 27, day 41, and day 55, respectively. X-axis: number of days on the respective diet. Y-axis: number of animals available on the day for *in vivo* examination. The curling arrow indicates removal by the end of the study on the day for harvesting the liver specimens.

were acclimated to laboratory conditions for a minimum of seven days when fed a standard rodent chow *ad libitum* (Laboratory Rodent Diet 5001, LabDiet, St Louis, MO, USA). The animals were allowed water *ad libitum* throughout the duration of the study. The 12 animals in each of the two phases were randomly divided with eight in the test group and four in the control group. The rats in the test group were fed a methionine-choline-deficient (MCD[23,24]) diet (Harlan Telkad — TD.90262) *ad libitum*. The control rats were fed an amino acid control diet *ad libitum* (Harlan Telkad — TD.130936). The two phases when combined produced a sample size of 8 for the control group and 16 for the MCD-treated group with subgroups differing in size and the level of steatosis induced. After initiation of the respective diets, three rats including one of the control group and two of the MCD-diet fed group were euthanized at randomly set time intervals of, respectively, 12 (phase-I), 13 (phase-II), 27 (phase-II), 28 (phase-I), 41 (phase-II), 49 (phase-I), 55 (phase-II), and 77 (phase-I) days, for histological sampling of the livers in the respective groups of control and MCD-diet fed rats. Rats were euthanized after undergoing per-SfS measurements. *In vivo* per-SfS measurements presented in this work were those performed on all animals at the baseline, on day 12 of phase-I combined with day 13 of phase-II, and upon the removal of all animals for histological sampling.

2.2. *Experimental procedures*

The experimental procedures for per-SfS of the rat liver *in vivo* with ultrasound guidance of the fiber-probe placement are illustrated in Fig. 2. The rat was surgically prepared under general anesthesia. After sonographic evaluation of the liver, a sterile, 22 or 20-gage 1.5 inch spinal needle (depending upon the availability) was inserted percutaneously into the liver under ultrasound guidance. After retracting the stylet of the needle, a sterile 320 μm single-fiber probe was inserted through the needle into liver parenchyma. The placement of the fiber probe into the parenchyma via the needle was monitored by ultrasound until the fiber tip extended a few millimeters beyond the beveled needle tip. Doppler ultrasound was also used to monitor that vasculature was not apparent in the vicinity of the fiber tip. After stabilizing the fiber placement, five repeated SfS measurements were acquired from each subject for offline model-based processing of the spectral parameters including the scattering power. After per-SfS measurements, the rats slated to continue in the study were recovered and returned to their cages for observation. After per-SfS measurements, a rat to be euthanized for harvesting liver specimens underwent a ventral midline incision that extended cranially through the xiphoid and diaphragmatic reflection into the thoracic cavity using a #10 scalpel blade and metzenbaum surgical scissors. A 20-gage needle with a 3 cc

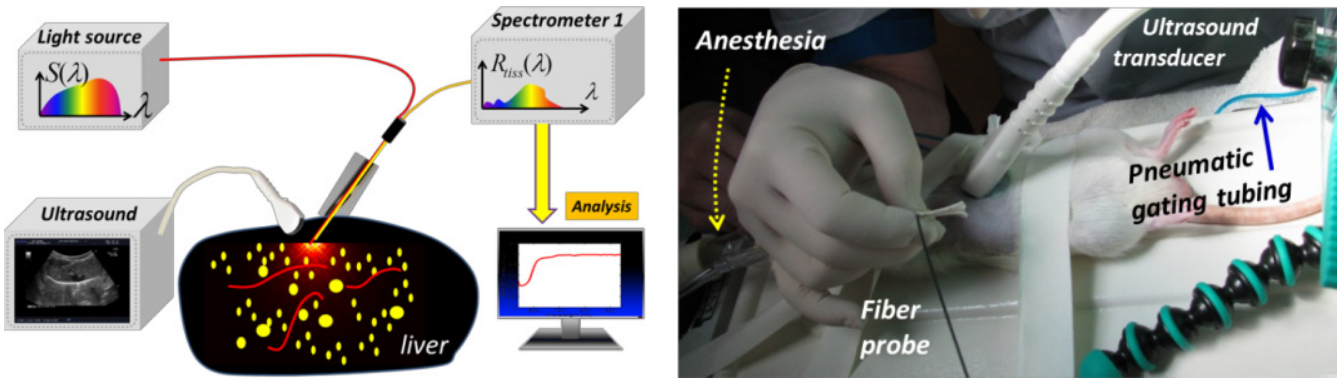

(a) (b)

Fig. 2. (a) The experimental configuration for percutaneous SfS of rat liver. A broadband light source and a compact VIS/NIR spectrometer were coupled, respectively, to one fiber branch (200 μm core) of a bifurcated fiber bundle. The combined terminal of the bifurcated fiber bundle (400 μm diameter) was connected to a 320 μm single-fiber applicator probe. The single-fiber probe was introduced into rat liver through a 22 (or 20) gage needle with ultrasound guidance. (b) A photograph of an anesthetized rat that underwent percutaneous SfS assessment of the liver with ultrasound monitoring of the fiber-probe placement. Marked in the photograph was also a small tubing connecting to a pneumatic pillow sensor placed at the left dorsal thoracic aspect of the rat for triggering SfS data acquisition at the same respiratory phase.

syringe was then used to collect ∼2 mL of whole blood by direct intracardiac puncture for biochemical analysis of plasma. Immediately following blood collection, direct intracardiac injection of 1 cc (390 mg) of pentobarbital sodium (Beuthansia D, Schering Plough, Union, New Jersey, USA) was administered for euthanasia. The body weight was measured immediately after euthanasia, followed by necropsy and harvesting of liver specimens. Tissue specimens were harvested from the right lobe of the excised liver by free-hand techniques. The specimens were harvested at arbitrary sites not correlated with the site of per-SfS, as it was not possible to accurately identify the site of *in vivo* per-SfS probing within the liver parenchyma when the liver was excised. The hepatic tissue specimens were fixed in 10% neutral buffered formalin, which does not cause false positive of lipid deposition in tissue.[25] The liver specimens were then prepared for hematoxylin/eosin (H&E) staining and Oil-Red-O staining.[26] The histology was examined on the H&E-stained and Oil-Red-O-stained specimens only. A total of eight H&E-stained specimens and four Oil-Red-O-stained specimens were examined for each liver. The H&E-stained sections were cut at 4 μm thickness. The Oil-Red-O-stained specimens were cut at 10 μm thickness. A board-certified pathologist (J. W. R.) blinded to the groups ranked the H&E and Oil-Red-O (for confirmation of lipid)-stained specimens based upon the percentage amount of hepatocytes showing lipid accumulation. The identification of each animal (controlled by K. E. B.) was also blinded to the operators of per-SfS (D. P. and N. S.) as well as ultrasound (G. R. H. and C. R. W.) until the necropsy examinations of all animals were completed.

2.3. *Biochemical analysis of plasma*

Plasma samples were analyzed in the clinical laboratory of the veterinary teaching hospital of Oklahoma State University using standard laboratory methods. The analysis reported included the following serum markers: albumin, globulin, total bilirubin (T-Bil), glucose, cholesterol, triglyceride, sodium, chloride, aspartate aminotransferase (AST), alanine aminotransferase (ALT), and alkaline phosphatase.

2.4. *Spectral analysis specific to per-SfS*

The systems and methods of per-SfS had been detailed in other studies.[27] The per-SfS system, including the broadband source, fiber-probe, and compact spectrometer, produced a working spectral response in a narrow 400 nm range over 540–940 nm, away from the Soret band of blood-related molecules such as porphyrins.[28] The spectral analysis for per-SfS follows the semi-empirical model detailed by Kanick *et al.*[29–32] and others[33,34] corresponding to single-fiber probing of a scattering medium by using a 15° angle-polished fiber. The SfS signal $R_{\text{tiss}}(\lambda)$, due exclusively to the tissue properties, after normalizing the raw signal using reference measurements, was[35]:

$$R_{\text{tiss}}(\lambda) = \eta_{\text{eff}}(1 + 1.26\exp[-2.59A\lambda^{-b}])\frac{0.10[A\lambda^{-b}]^{1.99}}{8.08 + 0.10[A\lambda^{-b}]^{1.99}} \cdot \exp\left\langle -\left\{ \begin{matrix} [\hat{\mu}_a^{\text{HbO}}(\lambda)\text{StO}_2 + \hat{\mu}_a^{\text{HbR}}(\lambda)(1-\text{StO}_2)][\text{HbT}] \\ +0.93[\hat{\mu}_a^{\text{Lip}}(\lambda)f_{\text{Lip}} + \hat{\mu}_a^{\text{Wat}}(\lambda)(1-f_{\text{Lip}})] \end{matrix} \right\} \right.$$
$$\left. \cdot \frac{0.60}{[A\lambda^{-b}]^{0.18}\langle 0.64 + 0.48\{[\hat{\mu}_a^{\text{HbO}}(\lambda)\text{StO}_2 + \hat{\mu}_a^{\text{HbR}}(\lambda)(1-\text{StO}_2)][\text{HbT}] + 0.93[\hat{\mu}_a^{\text{Lip}}(\lambda)f_{\text{Lip}} + \hat{\mu}_a^{\text{Wat}}(\lambda)(1-f_{\text{Lip}})]\}^{0.64}\rangle} \right\rangle, \quad (1)$$

where n_{eff} is an effective index of scattering intensity formed when all isolated constant terms are combined, A is the scattering amplitude, b is the scattering power, $\hat{\mu}_a^{\text{HbO}}(\lambda)$ and $\hat{\mu}_a^{\text{HbR}}(\lambda)$ are, respectively, the absorption coefficients of 1 μM oxyhemoglobin and 1 μM deoxyhemoglobin (values exported from the spectral panel of VirtualPhotonics[36]), StO_2 is the hemoglobin oxygen saturation, [HbT] is the total hemoglobin concentration (in μM), $\hat{\mu}_a^{\text{Lip}}(\lambda)$ and $\hat{\mu}_a^{\text{Wat}}(\lambda)$ are, respectively, the absorption coefficients of lipid and water at 1% volume fraction (values also exported from the spectral panel of VirtualPhotonics[36]), and f_{Lip} is the fraction of lipid in the water-lipid body. The fraction of water and lipid in tissue was assumed a constant value of 93% following studies specific to liver.[37] The pigment packaging effect[38] was implemented but was found insensitive as the Soret band

of blood-related molecules such as porphyrins was distant from the effective spectral response of the system. A nonlinear least-square fitting of the measurement data with Eq. (1) then estimated the parameters of interest.

2.5. *Morphometric particle analysis on the histology images*

The images of H&E-stained liver specimens were processed using ImageJ[39] for morphometric analysis of the area fraction, total count, and average size of the lipid droplets.[40] The steps of the morphometric analysis are outlined in Fig. 3. On an original colored H&E image (Panel A), the lipid droplets are clearly visualized as circular or slightly elliptical particles. The original colored H&E image was first converted to an 8-bit gray-scale image (Panel B), which was then black-white inverted so the lipid droplets would appear black (Panel C). The black-white inverted image was then applied an upper threshold (20 out of 255) of the gray scale to remove inter-hepatocyte structures not indicating lipid droplet features (Panel D), followed by particle analysis. All particles with the circularity between 0.5 and 1.0 and the diameter between 0.1 μm and 50 μm were counted (Panel E). The upper limit of the particle size was set at 50 μm, after gross examination of the largest lipid droplets on all specimens, for avoiding automated counting of some large structures that were not lipid droplets (e.g., the central vein). The analyses produced particle size distribution (Panel F), from which the total count of the particles and the average particle diameter were calculated, and the area fraction (%) occupied by the counted particles. Similar procedures were tested with the Oil-Red-O images, but the particle analyses with the Oil-Red-O images were found not as robust as with the H&E images, due to the limited color contrast of the acquired Oil-Red-O images. The Oil-Red-O images were thus used for confirming the extensity of the lipid accumulation as assessed on the H&E images, but not for deriving the particle morphometry.

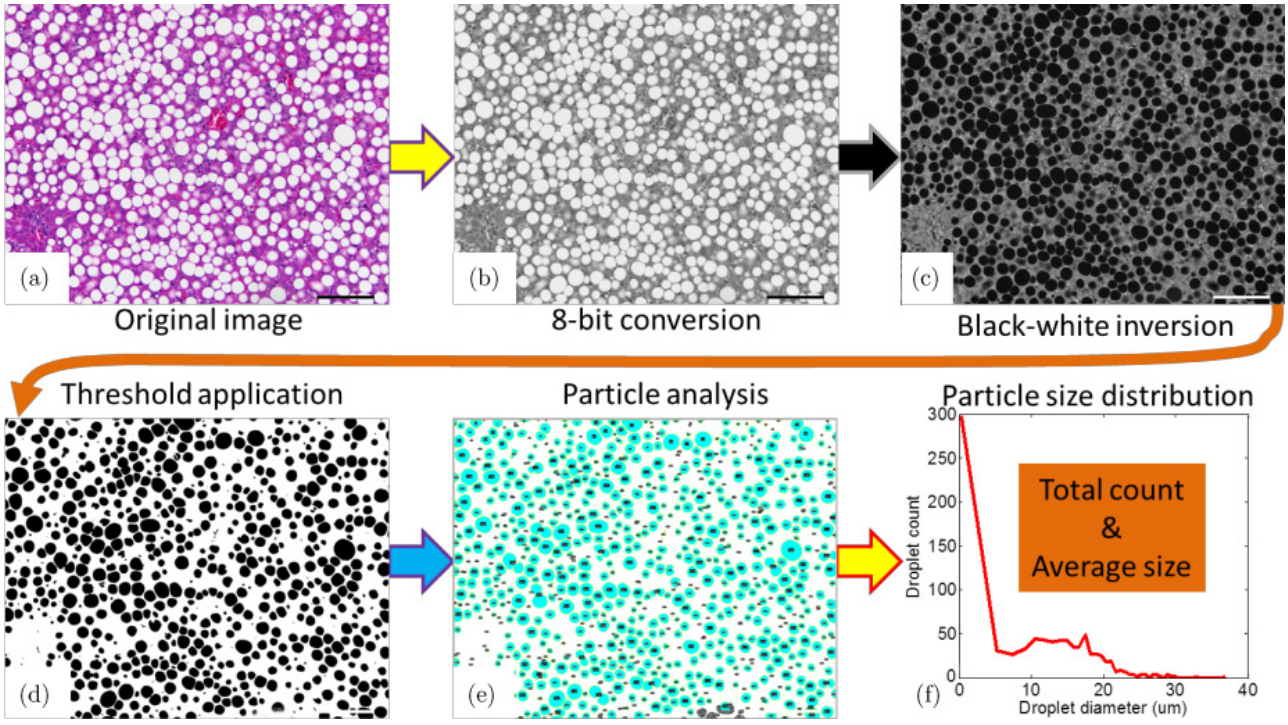

Fig. 3. Sequence of image processing by ImageJ for morphometric analysis of the lipid droplets. (a) The original colored image of H&E-stained liver specimen. (b) An 8-bit conversion of the colored image. (c) The black-white inverted image of the 8-bit image. (d) An upper threshold of the gray scale applied to the black-white image. (e) The counted particles are overlapped on the threshold applied image. (f) An example of the particle size histogram as the output of the particle analysis (X-axis: droplet diameter in μm; Y-axis: droplet count). Dimension of the bar on the histology image = 100 μm.

2.6. *Statistical analysis*

Statistical data analysis was performed with GraphPad Prism 6 (GraphPad Software, La Jolla, CA, USA). The groups compared had different sample sizes. The control group had a sample size of 8. The test group had a sample size of 16 when all were combined, or a sample size of 7, 3, or 6 depending on the pathologic level of hepatic steatosis. Paired t-test was applied to the same group at two different time-points to determine whether a specific parameter of the group changed over time. Mann–Whitney test was applied to two groups of different sample sizes to determine whether there was a difference of a specific parameter between two groups at the same time-point. One-way analysis of variance (ANOVA) was applied to three or more groups of data. $p < 0.05$ infers statistically significant difference.[41] The results were plotted as the mean value and the error bars that represent the standard deviation.

3. Results

3.1. *Ultrasound and per-SfS of representative levels of steatosis*

The representative results including transabdominal ultrasound and per-SfS of the rat livers with different levels of steatosis are presented in Fig. 4. The top row corresponds to the baseline ultrasound images of the rats on day 0. The second row displays the ultrasound images at the day of euthanasia. The third row is for the per-SfS measurements on the day of euthanasia. The per-SfS result of a test rat is plotted against that of a control rat euthanized on the same day. Shown in the fourth row are the images of H&E staining and the bottom row images of Oil-Red-O staining.

The column marked as "control" was from a control rat scarified on day 13. No droplet structures indicating lipid accumulation in hepatocytes were found in the H&E-stained and Oil-Red-O-stained specimens. For this control rat, the sonographic features of the liver on day 13 appeared normal as was on day 0. The per-SfS of this control liver resolved a scattering power of 0.035.

The column marked as "mild" was from an MCD-diet-treated rat scarified on day 13. Lipid infiltration in less than 30% of hepatocytes was found in the H&E-stained and Oil-Red-O-stained specimens, with an evident level of microvesicular steatosis. For this MCD-diet-treated rat with mild lipid accumulation, the sonographic features of the liver on day 13 were similar in echogenicity when compared with the day 0 livers. When comparing between the two per-SfS profiles, the spectral intensity of the one corresponding to the MCD-diet-treated liver declined with the wavelength increasing from $\sim$700 nm. The per-SfS of this MCD-treated liver resolved a scattering power of 0.33 in comparison to its control counterpart of 0.035.

The column marked as "moderate" was from an MCD-diet-treated rat euthanized on day 27. Lipid infiltration in greater than 30% but less than 60% of hepatocytes was found in the H&E-stained and Oil-Red-O-stained specimens. Microvesicular steatosis was present in this specimen, but at a much lesser amount when compared with that in the mildly infiltrated specimen. For this MCD-diet-treated rat with moderate lipid accumulation, the sonographic features of the liver on day 27 showed diffuse increased parenchymal echogenicity, development of hepatomegaly, some loss of visibility of hepatic vascular architecture and mild sound attenuation in the presence of echogenic liver, which together supported fatty liver diagnosis.[14] When comparing between the two per-SfS profiles, the spectral intensity of the one corresponding to the MCD-diet-treated liver declined with the wavelength increasing from $\sim$700 nm. The per-SfS of this MCD-diet-treated liver resolved a scattering power of 0.31 in comparison to its control counterpart of -0.33.

The column marked as "severe" was from an MCD-diet-treated rat euthanized on day 55. Lipid infiltration in greater than 60% of hepatocytes was found in the H&E-stained and Oil-Red-O-stained specimens. For this MCD-diet-treated rat with severe lipid accumulation, the sonographic features of the liver on day 55 presented marked sound attenuation leading to poor visualization of the diaphragm and hepatic vessels in addition to highly diffuse increased parenchymal echogenicity, which were diagnostic of fatty infiltration.[16] When comparing the per-SfS profile between the control rat and the MCD-diet-treated rat, the spectral intensity of the liver of the MCD-diet-treated rat was noticeably higher than that of the control rat, and the spectral intensity of it declined with the wavelength increasing from $\sim$700 nm. The per-SfS of this MCD-diet-treated liver resolved a scattering power of 0.55 in comparison to its control counterpart of 0.21.

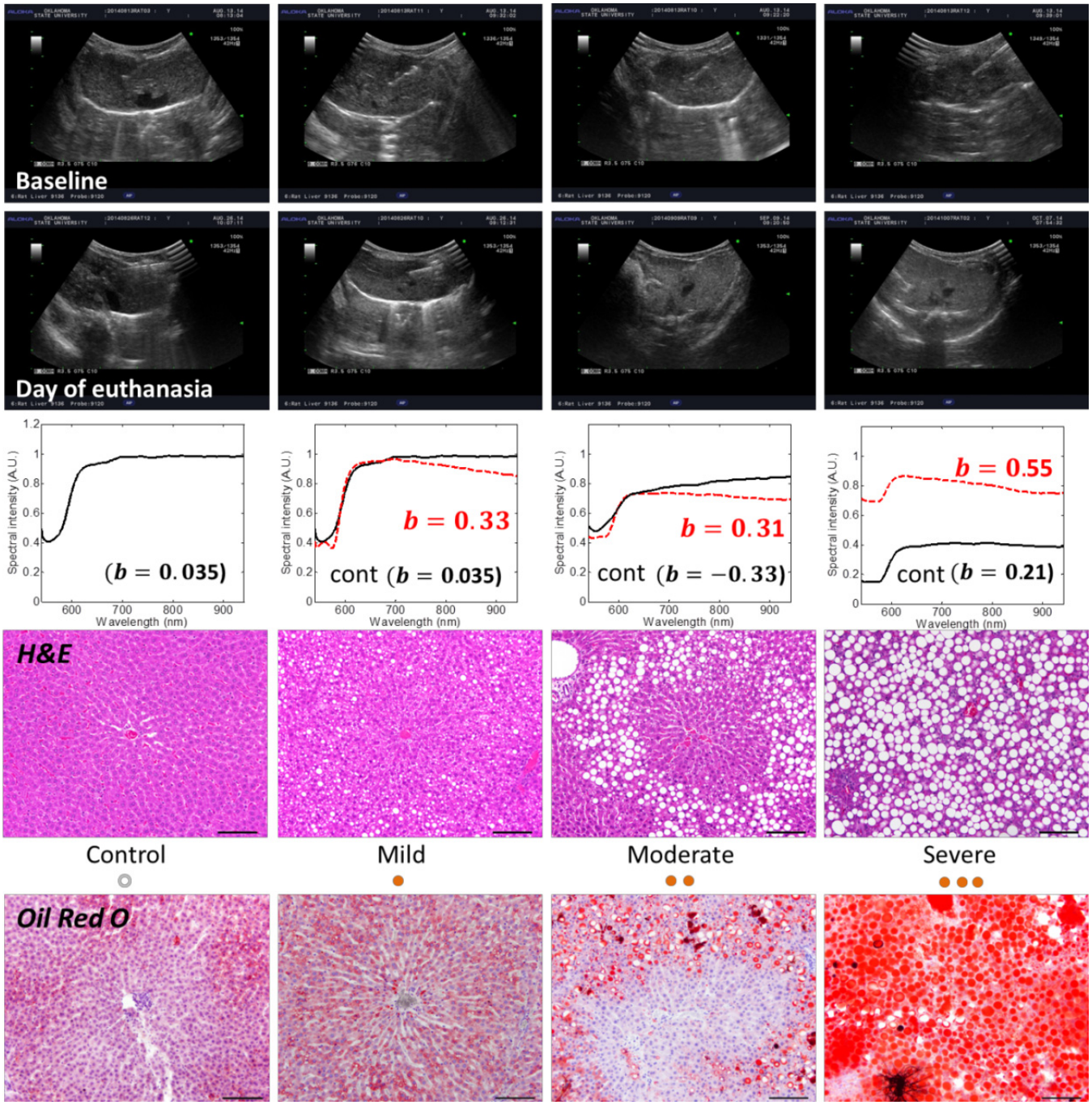

Fig. 4. Rows are counted from the top. Row (1): ultrasonography at the baseline. Row (2): ultrasonography at the day of euthanasia. Row (3): SfS profile taken at the day of euthanasia. X-axis: wavelength (nm); Y-axis: spectral intensity (arbitrary unit). Row (4): image of H&E-stained specimen. Row (5): image of Oil-Red-O-stained specimen. Columns are counted from the left. Column (1): The one marked as "control" below the H&E image was from a control rat of phase-II that was sacrificed on day 13. Column (2): The one marked as "mild" below the H&E image was from an MCD-diet-treated rat in phase-II that was sacrificed on day 13 (the same set of euthanasia including the control rat shown here as "control"). Column (3): The one marked as "moderate" below the H&E image was from an MCD-diet-treated rat in phase-II that was sacrificed on day 27. Column (4): The one marked as "severe" below the H&E image was from an MCD-diet-treated rat of phase-II that was sacrificed on day 55. Dimension of the bar on the histology image = 100 μm.

3.2. *Histopathological grading of the steatosis in all animals*

The pathologist's grading of the steatosis of the 24 livers (8 control and 16 MCD-diet-treated) after assessing both H&E- and Oil-Red-O-stained specimens is summarized in Fig. 5. The summary plot of the grading is also presented with representative Oil-Red-O images of the two MCD-diet-treated livers harvested on the near-2 week, near-4 week, near-6 week, near-8 week, and 11-week time-points of the study. All eight control livers were absent of lipid accumulation, regardless of the length on the control diet. All four MCD-diet-treated livers that were harvested at near-2 weeks presented mild lipid accumulation in the liver with various but evident amounts of microvesicular steatosis. Among the four MCD-diet-treated livers that were harvested at near-4 weeks, one presented mild lipid accumulation, two presented moderate lipid accumulation, and one presented severe lipid accumulation. Both of the two MCD-diet-treated livers that were harvested at near-6 weeks presented severe lipid accumulation. The two MCD-diet-treated livers that were harvested at 7 weeks presented mild lipid accumulation in one and severe lipid accumulation in the other. Both of the two MCD-diet-treated livers that were harvested at near-8 weeks presented severe lipid accumulation. The two MCD-treated livers that were harvested at 11 weeks presented mild lipid accumulation in one and moderate lipid accumulation in the other. The rats fed MCD diet did not exhibit any other significant hepatic pathology outside of what is reported here, i.e., primarily the fatty accumulation within the hepatocytes. There was neither significant inflammation nor fibrosis.

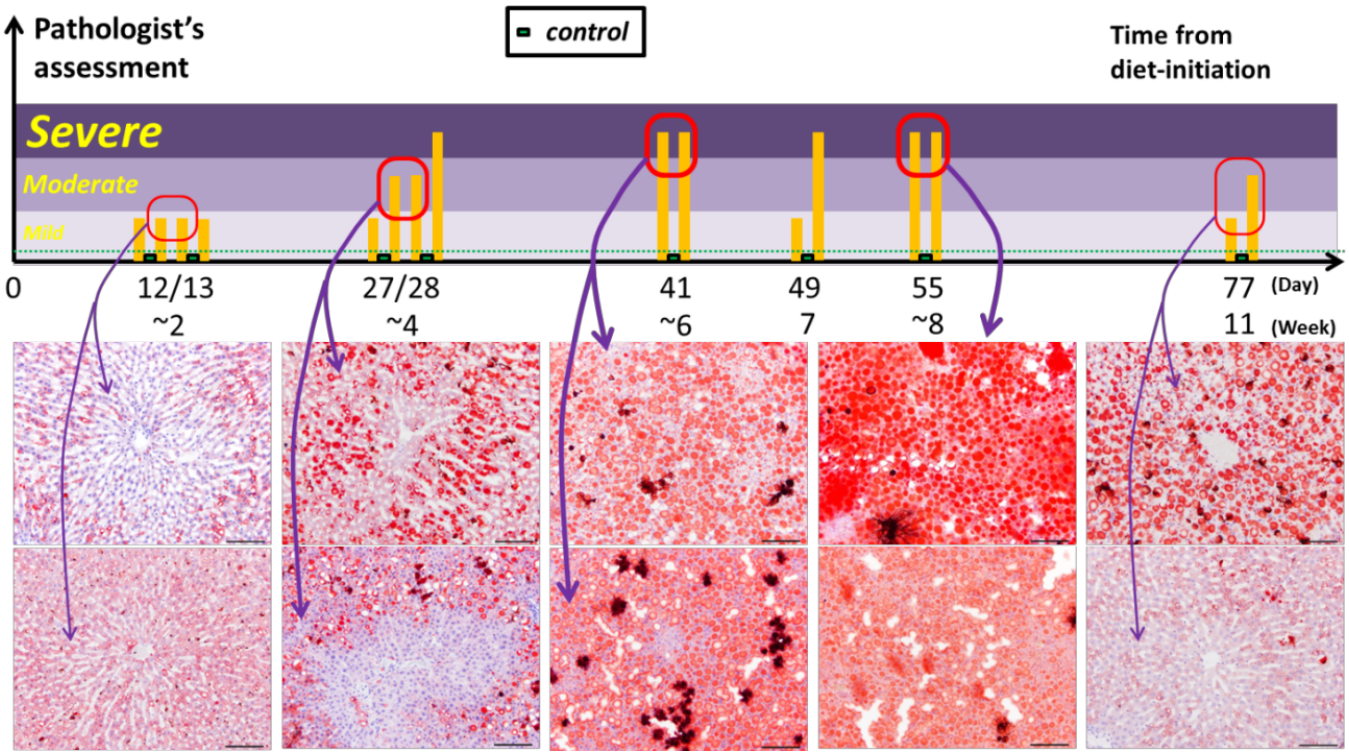

Fig. 5. Histological grading of the hepatic steatosis of the rats at different lengths of the diet intake. X-axis: length in days of diet intake; Y-axis: severity of steatosis. Two specimens were harvested at $\sim$2, $\sim$4, $\sim$6, $\sim$8, and 11 weeks, respectively. The upper panel with horizontal strips illustrates the severity of steatosis by color (three levels of the darkness, increased darkness for mild, moderate, and severe) or font size (three sizes of the font, increased font size for mild, moderate, and severe), versus the length of diet induction up to 77 days or 11 weeks. The lower panel shows two images of Oil-Red-O-stained liver specimens harvested, respectively, from two rats identified at the top panel that presented the level of steatosis marked by the red closed line. Dimension of the bar on the histology image = 100 μm.

3.3. *Lipid morphometry corresponding to the grade of steatosis and the length of diet intake*

The results of particle analysis on liver specimens absent of and presented with mild, moderate, and severe levels of steatosis are given in Fig. 6. The particle size distributions are plotted at the same scales, for particle diameters up to 30 μm and particle count up to 2000. The particle count is displayed at a logarithmic scale to magnify the changes occurring as larger droplets appearing at higher grade of steatosis. The dashed arrows on the figure indicate the same plot of the particle size distribution over its subsequent figure to be used as a reference to the particle sizes of the current specimen. When comparing the specimen of mild steatosis with the control one, the number of droplet of sub-μm size increased substantially and droplets of $\sim$10 μm size started to appear. When comparing the specimen of moderate steatosis with the one of mild steatosis, the number of droplet structures less than 8 μm in diameter decreased, but the number of droplet structures greater than 8 μm increased significantly, with the appearing of droplets as large as 20 μm. When comparing the specimen of severe steatosis with the one of moderate steatosis, the number of droplet structures less than 8 μm in diameter decreased, but the number of droplet structures greater than 8 μm increased significantly, with the appearing of droplets as large as 30 μm.

The morphometric results obtained from the H&E images of all 24 rats (8 control and 16 MCD-diet-treated) are displayed in Figs. 7(a) to 7(c) with respect to the terminal duration (in weeks) of each animal on its respective diet: (a) is the area fraction, (b) the total droplet count, and (c) the mean diameter of the droplet structures. The same

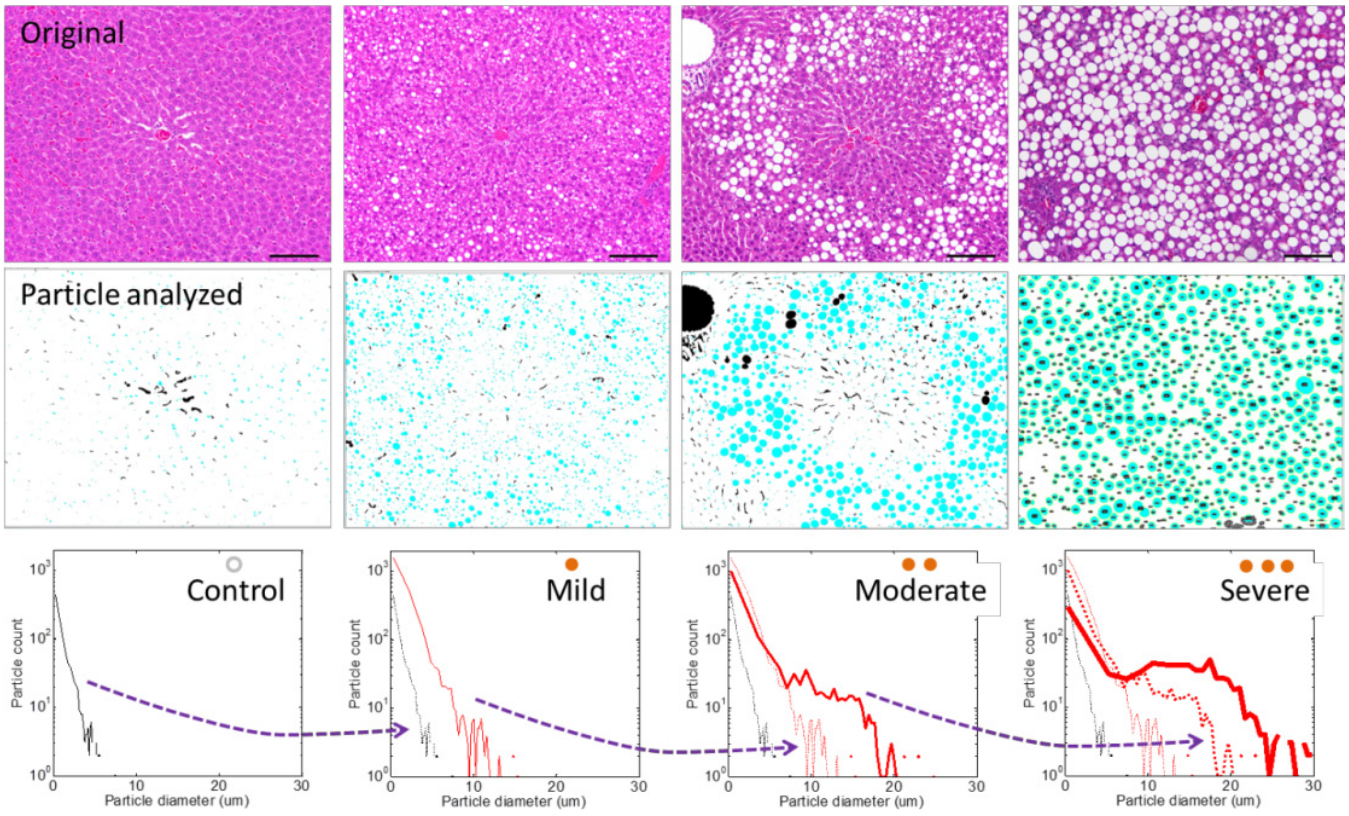

Fig. 6. The top row shows the images of the H&E-stained specimens at four levels of steatosis: control, mild, moderate, and severe. These four images are identical to those on row 4 of Fig. 4. The images at the middle row are the images at the top row after morphometric analysis to mark the lipid droplets, equivalent to (e) of Fig. 3. The bottom row displays the particle size distribution. X-axis: particle diameter (μm). Y-axis: particle count. The change from control to mild is presented with the appearance of primarily small particles (diameter <10 μm, the particle count increases logarithmically at smaller particle). The change from mild to moderate is presented with the appearance of particles of 10–20 μm. The change from moderate to severe is presented with continued increase of particles of 10–20 μm and the appearance of particles of sizes up to 30 μm. Dimension of the bar on the histology image = 100 μm.

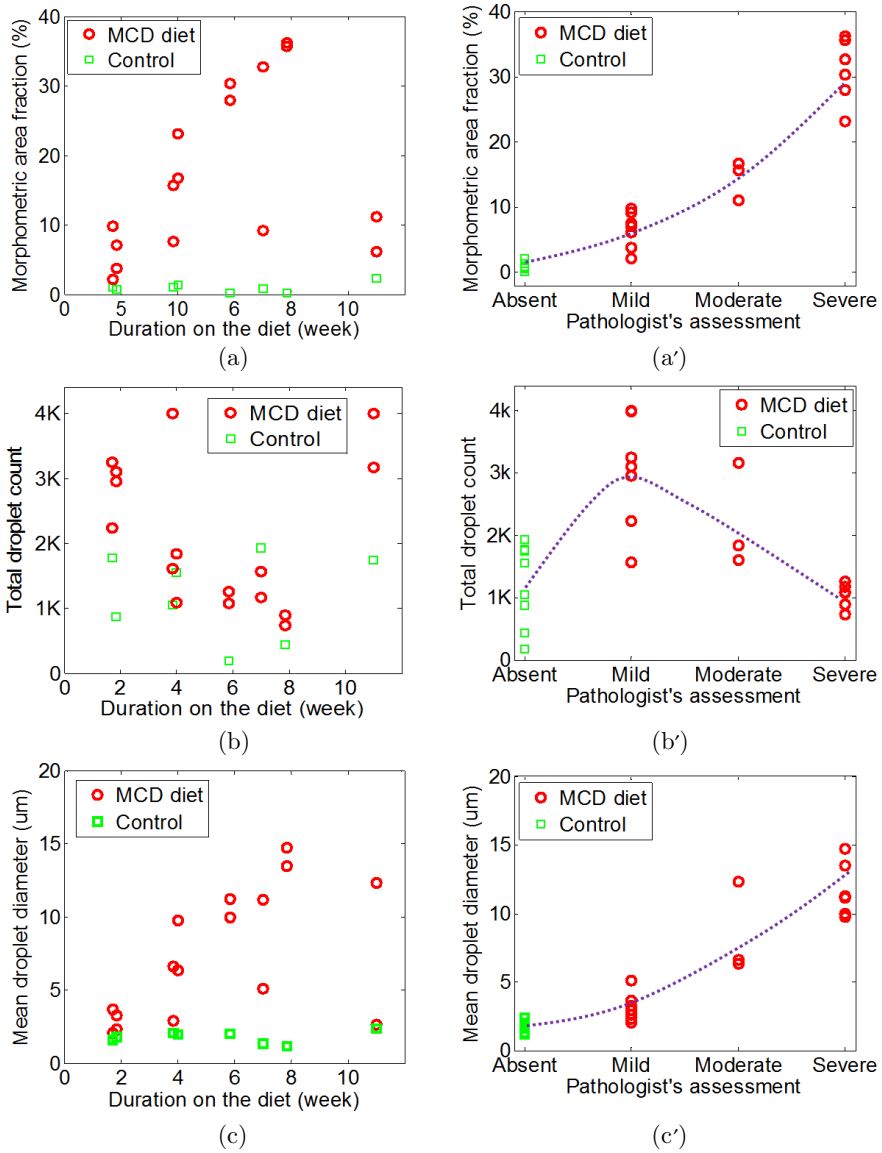

Fig. 7. (a) Area fraction with respect to the duration of the animal on the respective diet. (a′) Area fraction with respect to the pathological grade of steatosis. (b) Total count of the lipid droplet structures with respect to the duration of the animal on the respective diet. (b′) Total count of the lipid droplet structures with respect to the pathological grade of steatosis. (c) Average droplet size with respect to the duration of the animal on the respective diet. (c′) Average droplet size with respect to the pathological grade of steatosis. In all sub-figures, the green square represents control rat, and the red circle represents MCD-diet-treated rat.

morphometric analyses results are displayed in Figs. 7(a′) to 7(c′), with respect to the histopathologically assessed grade of the steatosis. The morphometric area fraction of the droplet structures in the control specimens ($n = 8$) ranged from 0.14% to 2.22%. The morphometric area fraction of the droplet structures in the mild MCD-diet-treated subset ($n = 7$) ranged from 2.12% to 9.76%. The morphometric area fraction of the droplet structures in the moderate MCD-diet-treated subset ($n = 3$) ranged from 5.90% to 16.69%. The morphometric area fraction of the droplet structures in the severe MCD-diet-treated subset ($n = 6$) ranged from 23.14% to 36.14%. The morphometric area fraction of the MCD-diet-treated livers, when plotted with respect to the length of diet intake as shown in (a), has shown to be generally higher if treated longer with the MCD diet up to 8 weeks. The area factions of the two rats examined at the 11 weeks were, however, significantly lower than

those examined at the 8 weeks. The mean droplet size as shown in (c) revealed patterns similar to those of the area fraction as in (a). The droplets were generally bigger if treated longer with the MCD diet over the first 8 weeks but were smaller at the 11-week time line when compared with those at the 8 weeks. When plotted with respect to the pathological grade of the steatosis, both the morphometric area (a′) and the mean droplet size (c′) were generally greater in samples with higher steatosis grade. The total count of the droplet structures, however, has shown an unclear pattern in (b) with respect to the duration on the diet and a clear bi-phasic pattern in (b′) with respect to the pathological grade of the steatosis. The total droplet count of specimens was substantially greater (more than two folds on average) in the specimens with mild steatosis when compared with the control specimens, but were less in the moderate steatosis when compared with the mild steatosis, and less in the severe steatosis when compared with the moderate steatosis. When the total droplet count of the MCD-diet-treated specimens was plotted against the morphometric area fraction as is shown in Fig. 8 (a), the total count was shown to be inversely proportional to the area fraction, agreeing with other reports for MCD-diet-induced hepatic steatosis in mice.[42] When the mean droplet diameter of the MCD-treated specimens was plotted against the morphometric area fraction as shown in (b), a linearity of $R = 0.93$ between the size and the area was established, indicating that higher steatosis grade is associated with bigger droplet size.

3.4. *Scattering power with respect to the grade of steatosis*

The distribution of the terminal scattering powers resolved by per-SfS for the 24 rats is presented in Fig. 9(a) according to the pathological grade of steatosis. The distribution in (a) is alternatively represented in (b) using bar-charts. The eight control livers presented a scattering power of 0.036 ± 0.25. The seven MCD-diet-treated livers with mild steatosis presented a scattering power of 0.25 ± 0.13. The three MCD-diet-treated livers with moderate pathological steatosis presented a scattering power of 0.48 ± 0.16. The six MCD-diet-treated livers with severe pathological steatosis presented a scattering power of 0.31 ± 0.29. These four groups of scattering power corresponded to a statistical power of $p = 0.0349$ (one-way ANOVA) that inferred a difference. The potential of the scattering power for detecting steatosis (giving a dichotomous diagnosis of either absence-of-steatosis or presence-of-steatosis) was assessed using the receiver-operating-characteristics (ROC) in (c) that analyzed the true positive fraction and false positive fraction at the scattering power varying between -0.2 and 0.5. An area-under-curve of 0.797 was obtained from the ROC curve. When the 16 MCD-diet-treated livers were combined as is shown by the framed part in (d) labeled with "Day last" that is also marked by an arrow from (b), they presented a scattering power (0.32 ± 0.21, $n = 16$) that was significantly greater ($p = 0.0189$) than that for the control livers (0.036 ± 0.25, $n = 8$). For these 24 samples, the pathological steatosis grades of them were all known.

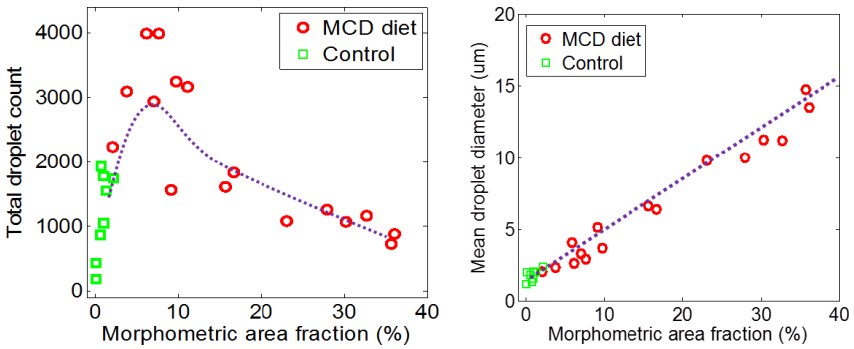

(a) (b)

Fig. 8. (a) Total count of the lipid droplet structures with respect to the area fraction. (b) Average droplet size with respect to the area fraction. In all sub-figures, the green square represents control rat, and the red circle represents MCD-diet-treated rat. In both figures, a hand-sketched broken line is used to illustrate the global pattern.

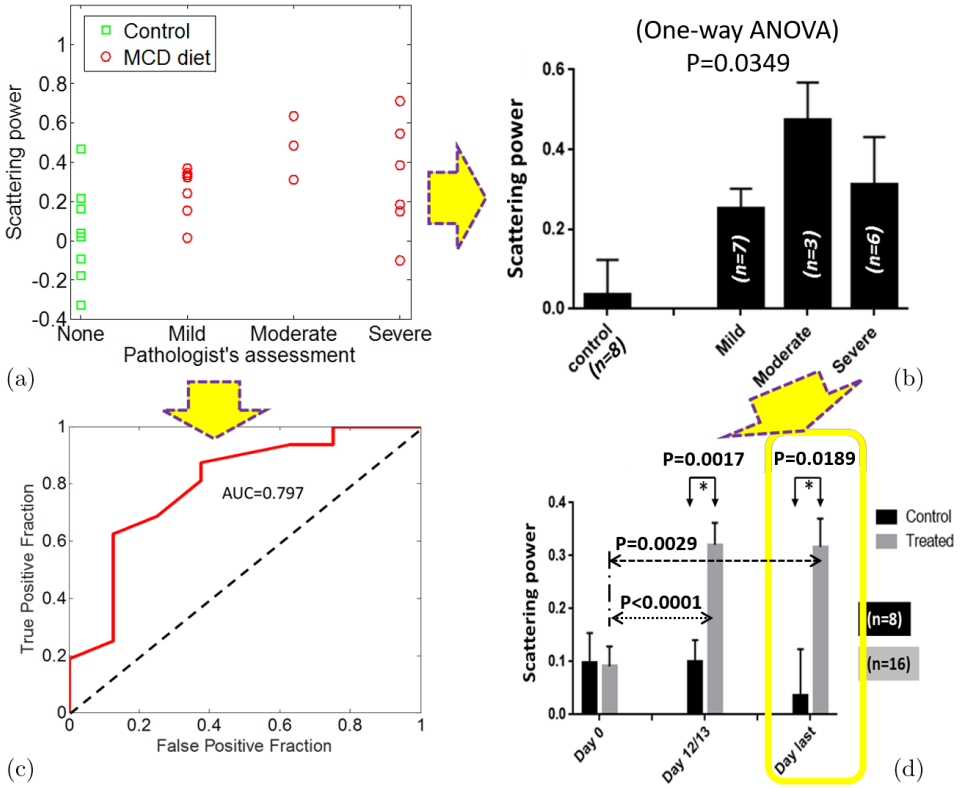

Fig. 9. (a) Distribution of the scattering power with respect to the pathological grade of steatosis. (b) The distribution of (a) presented as a bar-chart for the four subsets. (c) The ROC analysis results in an area-under-curve of 0.797 for using the scattering power to make the diagnosis of steatosis. (d) The scattering powers of the 8 rats in the control group and 16 in the MCD-diet-treated group, when evaluated on the day of initiating the respective diets, day 12/13 of two phases combined, and the day of euthanasia (bar charts: mean + standard deviation).

The scattering powers of the 24 rats on the day 12/13 timeline of the two phases combined were also compared in (d) with the label of "Day 12/13". For these 24 rats on the day 12/13 timeline, the pathological steatosis grades of only six livers (two control and four MCD-diet treated) were known. On day 12/13, the scattering power of the livers in the test group (0.32 ± 0.17, $n = 16$) was significantly elevated than ($p < 0.0017$) that of the control livers (0.10 ± 0.11, $n = 8$). The scattering powers of the 24 rats on the day of initiating their respective diets were also compared in (d) with the label of "Day 0". On day 0, the scattering power of the livers in the test group (0.09 ± 0.19, $n = 16$) and that of the control livers (0.10 ± 0.17, $n = 8$) were similar ($p = 0.93$). The change of the scattering power of the control group from day 0 to day 12 was not evident ($p = 0.22$) but that of the test group was significant ($p < 0.0001$). The change of the scattering power of the control group from day 0 to day of euthanasia was not evident ($p = 0.23$) but that of the test group was significant ($p = 0.0029$).

3.5. *Other outputs of the spectral analysis*

The total hemoglobin concentrations of 8 control rats and 16 test rats on day 0 were $441.6 \pm 48.0\,\mu$M and $410.9 \pm 50.0.5\,\mu$M, respectively ($p = 0.83$). The total hemoglobin concentrations of the 8 control rats and 16 test rats on the day of euthanasia were $458.8 \pm 79.1\,\mu$M and $334.3 \pm 53.8\,\mu$M, respectively ($p = 0.14$). The reduction of the total hemoglobin of the 16 test rats on the day of euthanasia in comparison to their respective baselines on day 0 was not significant ($p = 0.30$). No significant differences were found for the hemoglobin oxygenation when compared longitudinally within the same group or laterally between the control and MCD-diet-treated group. No significant differences were found for the effective scattering intensity when compared longitudinally within the same group or laterally between the control and MCD-diet-treated group. In summary, no significant difference was found in parameters other than the scattering power that

were retrieved from the per-SfS measurements, including total hemoglobin, hemoglobin oxygenation, water, lipid fraction, and effective scattering intensity, between the MCD-diet-treated group and the control group at the same time-point or between two time-points of the same group.

3.6. *Biochemical parameters*

Due to the missing of data log, the biochemical parameters were incomplete. Records of albumin, globulin, total bilirubin, glucose, cholesterol, sodium, chloride, AST, ALT, and ALK phosphatase were retrieved for 6 out of 8 rats in the control group and 12 out of 16 rats in the MCD-diet-treated group. Records of triglyceride were retrieved for 5 out of 8 rats in the control group and 10 out of 16 rats in the MCD-diet-treated group. The results are presented in Fig. 10, which also informs the body weight. Records of body weight upon necropsy were retrieved for 4 out of 8 rats in the control group and 8 out of 16 rats in the MCD-diet-treated group.

Plasma albumin was slightly increased in the MCD-fed rats with statistical significance ($p = 0.0027$). No change of plasma globulin was seen in the MCD-diet-treated rats. Plasma albumin was slightly increased in the MCD-fed rats with statistical significance ($p = 0.0027$). No changes of plasma glucose and cholesterol were seen in the MCD-diet-treated rats. Plasma triglyceride was reduced in the MCD-fed rats with statistical insignificance ($p = 0.27$). No changes of plasma sodium and chloride contents were seen in the MCD-diet-treated rats. Plasma AST was increased in the MCD-fed rats with statistical insignificance ($p = 0.12$). Plasma ALT was increased to nearly two folds in the MCD-fed rats ($p = 0.0097$). No change of plasma ALK phosphatase was seen in the MCD-fed rats. In addition to the biochemical parameters, the body weight was reduced in the MCD-fed rats ($p = 0.0040$).

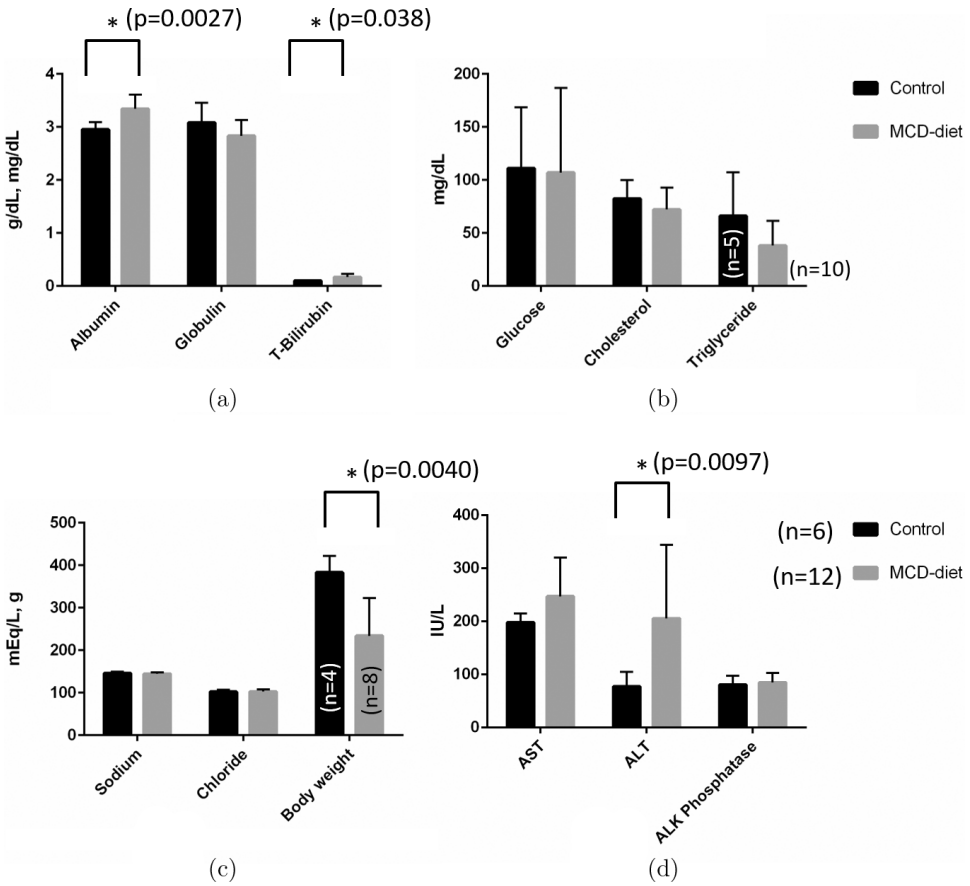

Fig. 10. Biochemical analyses of the plasma and body weight upon euthanasia. (a) Albumin (g/dL), globulin (g/dL), and total-bilirubin (mg/dL). (b) Glucose, cholesterol, and triglyceride (all mg/dL). (c) Sodium and chloride (mEq/L) and body weight (g). (d) AST, ALT, and ALK phosphatase (all IU/L). Sample sizes: $n = 6$ for the control group and $n = 12$ for the MCD-diet-treated group, unless noted directly on the bar chart.

4. Discussion

The scattering power resolved for the control livers is 0.1, a number that is in close agreement with the number reported for liver by van Leeuwen-van Zaane *et al.*[34] Among the 16 rats fed MCD diet, 7 had mild lipid accumulation, 3 had moderate lipid accumulation, and 6 had severe lipid accumulation. The scattering powers of the livers with pathological steatosis were all substantially greater than those of the control livers. Within the MCD-diet-treated group, the scattering power was higher in moderate than in mild subsets, but lower in the severe than in the moderate subsets. The pattern of change of the scattering power was projected to be caused by an initial accumulation of primarily small lipid droplets prior to the lipid droplets increasing in size.[35] In the previous report of reflectance spectroscopy,[35] it was demonstrated in simulation that an increase of 1 μm lipid droplet from 1% to 15% concentration in a lean liver could increase the scattering power from 0.1 of the lean liver to 0.13 and 0.31, and an increased lipid size from 2 μm to 25 μm at the same 33% volume concentration could cause the scattering power to decrease from 0.30 to 0.19. Such postulated changes of the lipid droplets are in agreement with the global changes of the lipid droplets as analyzed on the histopathological images in this present study containing both phases of the study. As shown in Fig. 6, the change from lean liver to liver with mild steatosis was associated with a substantial increase of smaller sub-μm size lipid droplets. As the steatosis elevated in grade, the number of smaller droplets decreased, but larger droplets with diameters ranging from 8 μm to 20–30 μm increased significantly. These morphometrically analyzed changes of the lipid droplet size also agreed with the patterns reported by Veteläinen *et al.*[43] from similar rat modeling work.

It is shown that the morphometric area fraction determined by the automated image analysis correlates well with the visual estimation of the liver steatosis by a pathologist, but the area fraction determined by the automated image analysis is systematically lower than that by the pathologist's visual estimation of the amount of number of hepatocytes with the presence of lipid infiltration. For example, on evaluation of specimens which had pathologically severe ($>60\%$) steatosis ($n = 6$), the automated morphometric analysis returned an area fraction ranging between 23.14% and 36.14%. On evaluation of specimens which had pathologically moderate (30%–60%) steatosis ($n = 3$), the automated morphometric analysis returned an area fraction ranging between 5.90% and 16.69%. On evaluation of specimens which had pathologically mild ($<30\%$) steatosis ($n = 7$), the automated morphometric analysis returned an area fraction ranging between 2.12% and 9.76%. On evaluation of specimens which were pathologically absent ($<5\%$) of steatosis ($n = 8$), the automated morphometric analysis returned an area fraction ranging between 0.14% and 2.22%. Similar discrepancies between the objectively identified and subjectively estimated lipid area fractions were reported by Marsman *et al.*[44] who compared the average percentage of fat content in 49 biopsy specimens analyzed by automated software and a trained pathologist. It was reported that the macrovesicular fat content of donor liver specimens determined by the pathologist was 2.9-fold greater, on average, than that obtained by the automated software.[44] Similarly, the pathologist's determination of total fat content was 1.4-fold greater, on average, than that obtained by the automated software.[44] The difference between the visual estimation of steatosis grade and automated quantitation of the fat fraction is caused in part by the difference between how a pathologist evaluates and how an automated image analysis performs. A pathologist determines the steatosis grade based on the subjective evaluation of the fraction of the hepatocytes infiltrated by lipid, whereas what an automated software toolbox calculates is the area fraction of the lipid droplets over the total image area. The area fraction extracted from a two-dimensional image by using the automated image analysis package was used directly in this study for keeping it consistent with the subjective estimation by the pathologist of the number of hepatocytes affected on a two-dimensional image. Should the lipid fraction be represented as the volume fraction,[16,44] the percentage values of the lipid content could have been even smaller. But the absolute values of the lipid fraction will not have affected the proportionality that it has with respect to either the lipid droplet size or count.

Several limitations are noted in this study that replied upon longitudinal assessments of the rat livers *in vivo* using per-SfS to identify a potential spectroscopic marker of steatosis development. One concern was that liver specimens obtained from three rats (two MCD and one control) might not

represent histological sampling for the whole experimental group at a given time-point. This was particularly concerning for sampling the experimental groups several weeks after the diet induction when the randomly selected animals could have the highest or lowest level of steatosis among the group at the stage of experiment. However, the under-sampling of the histology at a given time-point did NOT affect the evaluation of the histology of the whole group at the respective end-points (euthanasia). The under-sampling of the histology at a given time-point could have affected the evaluation at day 12/13 when 6 rats out of 24 rats (or 4 out of 18 MCD-diet-treated rats) were sampled. For the evaluation on day 12/13, the duration of the diet intake was relatively short at the near-2 weeks time-point and mild lipid infiltration was found in all of the four MCD-diet-fed rats. Therefore, it was a reasonable projection that all of the 16 MCD-diet-fed rats would have had mild lipid infiltration at that time-point, which, however, could not be confirmed. We note that there is no easy way both to accurately sample the histology of the (small) rat livers of the whole group and to longitudinally study the changes expected for the whole group over time.

Another limitation of the study was that direct intra-parenchymal sampling of the liver tissue by the single-fiber probe involved a tissue probing geometry that was better represented by the infinite-medium geometry than a semi-infinite medium geometry, but the current empirical models of single-fiber spectroscopy were available for a semi-infinite geometry only.[29–35] The discrepancy between the model geometry and the actual geometry could affect the spectral analysis of the intensity values, even though it may not change the relative pattern of the scattering spectra that is eventually dictated by the difference in the scattering powers. Thirdly, percutaneous fiber application could have caused injuries to the liver and confounded comparison at different time-points. However, artifacts due to the injury would occur in both control and test groups; therefore, it should not adversely affect the comparison between the control and test groups at the same time-points (i.e., day 12/13). Fourthly, the transabdominal evaluation of the fatty liver conditions with sonography was based on the gray-scale features only; so the steatosis diagnosis was likely not as sensitive as would have been obtained with other diagnostic imaging markers such as using the hepato-renal index.[12,13] Regardless of the diagnostic method used, the low sensitivity of ultrasonography in detecting a mild level of steatosis is however not unexpected. The lipid droplets formed during the initial stage of fatty infiltration could be one to two orders smaller than the ultrasonic wavlength in tissue. At a small lipid fraction of the total tissue during the onset of steatosis, the dispersed amount of the small lipid droplets could not change the acoustic impedance of the tissue sufficiently to increase the echogenicity. Lastly, the sampling of liver tissue in this study was done in a minimally invasive approach that would be less applicable than a non-invasive approach for clinical translation. The objective of this study was to discover a spectral feature that represented the "authentic" conditions of the liver over the course of diet intake, which was difficult to assess by noninvasive optical spectroscopy methods. It should be noted that it is possible to use surface-based reflectance spectroscopy applied directly with transabdominal reflectance spectroscopy to assess the scattering spectral feature, but that requires additional modeling or device technologies to compensate the effect of cutaneous and subcutaneous tissue by using methods such as multiple source–detector pairs[45] for the DRS.

A lasting limitation involving MCD-diet model is that MCD-diet-induced fatty infiltration in liver does not represent accurately the biology of human nonalcoholic fatty liver disease (NAFLD).[46] Although this model could replicate the histological features of liver injury as observed in human NAFLD, its metabolic context is distinct from human NAFLD, since animals fed the MCD diet lost weight [Fig. 10(c)] and presented decreased blood triglyceride and cholesterol, creating a metabolic profile opposite to the human disease. The main advantages of the MCD diet are that it is widely available and reliably replicates NAFLD histology within a relatively shorter feeding time than other dietary models of NAFLD. The histological relevance of MCD diet induction in terms of the fatty infiltration in liver has made it possible for this study to observe the changes of the scattering power and to associate the changes of the scattering power with the changes in the morphology of the lipid droplets in the liver.

5. Conclusions

In vivo per-SfS was performed on livers of rats fed MCD diet in comparison to control livers over

randomized intervals. The rats in the MCD-diet-treated group developed various levels of steatosis (seven of mild, three of moderate, and six of severe), relative to none in the control group ($n = 8$). Images of hematoxylin & eosin-stained specimens were also analyzed morphometrically to extract the area fraction, total count, and mean size of the lipid droplet structures. The mean droplet size increased linearly with the increase of the lipid area fraction, but the total count followed a bi-phasic pattern with the increase of the lipid area fraction. The per-SfS-resolved scattering power for the MCD-diet-treated livers (0.33 ± 0.21, $n = 16$) was significantly ($p < 0.0189$) greater than that for the control livers (0.036 ± 0.25, $n = 8$). When measured at near-2 weeks (day 12/13) with none of the MCD-diet-treated livers presenting steatosis-diagnostic patterns on sonography but all four specimens of the MCD-diet-treated group had pathological mild lipid infiltration with evident level of microvesicular steatosis, the per-SfS-resolved scattering power of the MCD-diet-treated livers (0.32 ± 0.17, $n = 16$) was significantly ($p = 0.0017$) greater than that of the control livers (0.10 ± 0.11, $n = 8$). The elevation of scattering power is shown to indicate the onset of steatosis in rat livers when the steatosis was not detected by ultrasound.

Conflict of Interest

The authors declare no conflict of interest with this manuscript.

Acknowledgments

The authors thank Dr Jim Meinkoth for assessing the biochemical parameters. This work was supported by a health search grant HR11-043 from the Oklahoma Center for the Advancement of Science and Technology (OCAST) and in part by the Kerr Foundation. This work was performed when Ms. Nigar Sultana was with the Graduate Program on Interdisciplinary Sciences, Oklahoma State University, Stillwater, OK 74078, USA. Currently, Ms. Nigar Sultana is with P3 Group, Southfield, MI 48034, USA.

References

1. Y. Soejima, M. Shimada, T. Suehiro, K. Kishikawa, T. Yoshizumi, K. Hashimoto, R. Minagawa, S. Hiroshige, T. Terashi, M. Ninomiya, S. Shiotani, N. Harada, K. Sugimachi, "Use of steatotic graft in living-donor liver transplantation," *Transplantation* **76**(2), 344–348 (2003).
2. W. R. Kim, J. R. Lake, J. M. Smith, M. A. Skeans, D. P. Schladt, E. B. Edwards, A. M. Harper, J. L. Wainright, J. J. Snyder, A. K. Israni, B. L. Kasiske, "OPTN/SRTR 2013 Annual Data Report: Liver," *Am. J. Transplant* **15**(Suppl. 2), 1–28 (2015), doi: 10.1111/ajt.13197.
3. L. De Carlis, C. V. Sansalone, G. F. Rondinara, G. Colella, A. O. Slim, O. Rossetti, P. Aseni, A. Della Volpe, L. S. Belli, A. Alberti, R. Fesce, D. Forti, "Is the use of marginal donors justified in liver transplantation? Analysis of results and proposal of modern criteria," *Transpl. Int.* **9**, S414–S417 (1996).
4. T. M. Fishbein, M. I. Fiel, S. Emre, O. Cubukcu, S. R. Guy, M. E. Schwartz, C. M. Miller, P. A. Sheiner, "Use of livers with microvesicular fat safely expands the donor pool," *Transplantation* **64**, 248–251 (1997).
5. F. Zamboni, A. Franchello, E. David, G. Rocca, A. Ricchiuti, B. Lavezzo, M. Rizzetto, M. Salizzoni, "Effect of macrovescicular steatosis and other donor and recipient characteristics on the outcome of liver transplantation," *Clin. Transpl.* **15**(1), 53–57 (2001).
6. H. Kato, N. Kuriyama, S. Duarte, P. A. Clavien, R. W. Busuttil, A. J. Coito, "MMP-9 deficiency shelters endothelial PECAM-1 expression and enhances regeneration of steatotic livers after ischemia and reperfusion injury," *J. Hepatol.* **60**(5), 1032–1039 (2014).
7. S. Nagai, Y. Fujimoto, H. Kamei, T. Nakamura, T. Kiuchi, "Mild hepatic macrovesicular steatosis may be a risk factor for hyperbilirubinaemia in living liver donors following right hepatectomy," *Br. J. Surg.* **96**(4), 437–444 (2009), doi: 10.1002/bjs.6479.
8. M. J. Lee, P. Bagci, J. Kong, M. B. Vos, P. Sharma, B. Kalb, J. H. Saltz, D. R. Martin, N. V. Adsay, A. B. Farris, "Liver steatosis assessment: Correlations among pathology, radiology, clinical data and automated image analysis software," *Pathol. Res. Pract.* **209**(6), 371–379 (2013), doi: 10.1016/j.prp.2013.04.001.
9. H. Yersiz, C. Lee, F. M. Kaldas, J. C. Hong, A. Rana, G. T. Schnickel, J. A. Wertheim, A. Zarrinpar, V. G. Agopian, J. Gornbein, B. V. Naini, C. R. Lassman, R. W. Busuttil, H. Petrowsky, "Assessment of hepatic steatosis by transplant surgeon and expert pathologist: A prospective, double-blind evaluation of 201 donor livers," *Liver Transpl.* **19**(4), 437–449 (2013), doi: 10.1002/lt.23615. Epub 2013 March 17.
10. A. R. Teixeira, M. Bellodi-Privato, J. B. Carvalheira, V. F. Pilla, J. C. Pareja, L. A. D'Albuquerque,

"The incapacity of the surgeon to identify NASH in bariatric surgery makes biopsy mandatory," *Obes. Surg.* **19**(12), 1678–1684 (2009), doi: 10.1007/s11695-009-9980-x.

11. J. R. van Werven, H. A. Marsman, A. J. Nederveen, N. J. Smits, F. J. ten Kate, T. M. van Gulik, J. Stoker, "Assessment of hepatic steatosis in patients undergoing liver resection: Comparison of US, CT, T1-weighted dual-echo MR imaging, and point-resolved 1H MR spectroscopy," *Radiology* **256**(1), 159–168 (2010), doi: 10.1148/radiol. 10091790.
12. S. Zelber-Sagi, M. Webb, N. Assy, L. Blendis, H. Yeshua, M. Leshno, V. Ratziu, Z. Halpern, R. Oren, E. Santo, "Comparison of fatty liver index with noninvasive methods for steatosis detection and quantification," *World J. Gastroenterol.* **19**(1), 57–64 (2013), doi: 10.3748/wjg.v19.i1.57.
13. A. Chauhan, L. R. Sultan, E. E. Furth, L. P. Jones, V. Khungar, C. M. Sehgal, "Diagnostic accuracy of hepatorenal index in the detection and grading of hepatic steatosis," *J. Clin. Ultrasound* **44**(9), 580–586 (2016), doi: 10.1002/jcu.22382.
14. A. J. Hessheimer, D. Parramón, A. Guimerà, I. Erill, A. Rimola, J. C. García-Valdecasas, R. Villa, C. Fondevila, "A rapid and reliable means of assessing hepatic steatosis in vivo via electrical bioimpedance," *Transplantation* **88**(5), 716–722 (2009), doi: 10.1097/TP.0b013e3181b391c0.
15. G. Xu, Z. X. Meng, J. D. Lin, J. Yuan, P. L. Carson, B. Joshi, X. Wang, "The functional pitch of an organ: Quantification of tissue texture with photoacoustic spectrum analysis," *Radiology* **271**(1), 248–254 (2014), doi: 10.1148/radiol.13130777.
16. D. J. Evers, A. C. Westerkamp, J. W. Spliethoff, V. V. Pully, D. Hompes, B. H. Hendriks, W. Prevoo, M. L. van Velthuysen, R. J. Porte, T. J. Ruers, "Diffuse reflectance spectroscopy: Toward real-time quantification of steatosis in liver," *Transpl. Int.* **28**(4), 465–474 (2015), doi: 10.1111/tri.12517. Epub 2015 January 21.
17. A. C. Westerkamp, V. V. Pully, G. Karimian, F. Bomfati, Z. J. Veldhuis, J. Wiersema-Buist, B. H. Hendriks, T. Lisman, R. J. Porte, "Diffuse reflectance spectroscopy accurately quantifies various degrees of liver steatosis in murine models of fatty liver disease," *J. Transpl. Med.* **13**, 309 (2015), doi: 10.1186/s12967-015-0671-1.
18. J. H. Nilsson, N. Reistad, H. Brange, C. F. Öberg, C. Sturesson, "Diffuse reflectance spectroscopy for surface measurement of liver pathology," *Eur. Surg. Res.* **58**(1–2), 40–50 (2017), doi: 10.1159/000449378.
19. T. Kitai, B. Beauvoit, B. Chance, "Optical determination of fatty change of the graft liver with near-infrared time-resolved spectroscopy," *Transplantation* **62**, 642–647 (1996).
20. B. L. McLaughlin, A. C. Wells, S. Virtue, A. Vidal-Puig, T. D. Wilkinson, C. J. Watson, P. A. Robertson, "Electrical and optical spectroscopy for quantitative screening of hepatic steatosis in donor livers," *Phys. Med. Biol.* **55**(22), 6867–6879 (2010).
21. D. A. Fabila-Bustos, U. D. Arroyo-Camarena, M. D. López-Vancell, M. A. Durán-Padilla, I. Azuceno-García, S. Stolik-Isakina, E. Ibarra-Coronado, B. Brown, G. Escobedo, J. M. de la Rosa-Vázquez, "Diffuse reflectance spectroscopy as a possible tool to complement liver biopsy for grading hepatic fibrosis in paraffin-preserved human liver specimens," *Appl. Spectrosc.* **68**(12), 1357–1364 (2014), doi: 10.1366/14-07462. Epub 2014 November 1.
22. A. Cerussi, D. Hsiang, N. Shah, R. Mehta, A. Durkin, J. Butler, B. J. Tromberg. "Predicting response to breast cancer neoadjuvant chemotherapy using diffuse optical spectroscopy," *Proc. Natl Acad. Sci. USA* **104**(10), 4014–4019 (2007). Epub 2007 February 28.
23. H. Itagaki, K. Shimizu, S. Morikawa, K. Ogawa, T. Ezaki, "Morphological and functional characterization of non-alcoholic fatty liver disease induced by a methionine-choline-deficient diet in C57BL/6 mice," *Int. J. Clin. Exp. Pathol.* **6**(12), 2683–2696 (2013). eCollection 2013.
24. J. Lin, F. Lu, W. Zheng, S. Xu, D. Tai, H. Yu, Z. Huang. "Assessment of liver steatosis and fibrosis in rats using integrated coherent anti-Stokes Raman scattering and multiphoton imaging technique," *J. Biomed. Opt.* **16**(11), 116024 (2011), doi: 10.1117/1.3655353.
25. W. J. Howat, B. A. Wilson, "Tissue fixation and the effect of molecular fixatives on downstream staining procedures," *Methods* **70**(1), 12–19 (2014).
26. W. Wilson, "A trichrome method for staining fat with oil red O in frozen sections," *Bull. Int. Assoc. Med. Mus.* **31**, 216–220 (1950).
27. D. Piao, K. L. McKeirnan, Y. Jiang, M. A. Breshears, K. E. Bartels, "A low-cost needle-based single-fiber spectroscopy method to probe scattering changes associated with mineralization in canine intervertebral disc," *Photon. Lasers Med.* **1**(2), 103–115 (2012).
28. D. Piao, K. L. McKeirnan, N. Sultana, M. A. Breshears, A. Zhang, K. E. Bartels, "Percutaneous single-fiber reflectance spectroscopy of canine intervertebral disc: Is there a potential for in situ probing of mineral degeneration?" *Lasers Surg. Med.* **46**(6), 508–519 (2014), doi: 10.1002/lsm.22261. Epub 2014 June 1.d.
29. S. C. Kanick, H. J. C. M. Sterenborg, A. Amelink, "Empirical model of the photon path length for a

single fiber reflectance spectroscopy device," *Opt. Exp.* **17**(2), 860–871 (2009).
30. S. C. Kanick, D. J. Robinson, H. J. C. M. Sterenborg, A. Amelink, "Monte Carlo analysis of single fiber reflectance spectroscopy: photon path length and sampling depth," *Phys. Med. Biol.* **54**(22), 6991–7008 (2009).
31. S. C. Kanick, U. A. Gamm, M. Schouten, H. J. C. M. Sterenborg, D. J. Robinson, A. Amelink, "Measurement of the reduced scattering coefficient of turbid media using single fiber reflectance spectroscopy: Fiber diameter and phase function dependence," *Biomed. Opt. Exp.* **2**, 1687–1702 (2011).
32. S. C. Kanick, U. A. Gamm, H. J. C. M. Sterenborg, D. J. Robinson, A. Amelink, "Method to quantitatively estimate wavelength-dependent scattering properties from multidiameter single fiber reflectance spectra measured in a turbid medium," *Opt. Lett.* **36**, 2997–2999 (2011).
33. U. A. Gamm, S. C. Kanick, H. J. C. M. Sterenborg, D. J. Robinson, A. Amelink, "Quantification of the reduced scattering coefficient and phase-function-dependent parameter γ of turbid media using multidiameter single fiber reflectance spectroscopy: Experimental validation," *Opt. Lett.* **37**, 1838–1840 (2012).
34. F. van Leeuwen-van Zaane, U. A. Gamm, P. B. van Driel, T. J. Snoeks, H. S. de Bruijn, A. van der Ploeg-van den Heuvel, I. M. Mol, C. W. Löwik, H. J. Sterenborg, A. Amelink, D. J. Robinson, " *In vivo* quantification of the scattering properties of tissue using multi-diameter single fiber reflectance spectroscopy," *Biomed. Opt. Exp.* **4**(5), 696–708 (2013).
35. D. Piao, N. Sultana, G. R. Holyoak, J. W. Ritchey, C. R. Wall, J. K. Murray, K. E. Bartels, " *In vivo* assessment of diet-induced rat hepatic steatosis development by percutaneous single-fiber spectroscopy detects scattering spectral changes due to fatty infiltration," *J. Biomed. Opt.* **20**(11), 117002 (2015), doi: 10.1117/1.JBO.20.11.117002.
36. VirtualPhotonics Technology Initiative, http://www.virtualphotonics.org/software. Accessed on September 2, 2017. This open source resource was made possible in part by the Laser Microbeam and Medical Program (LAMMP: P41 EB015890-33), an NIH/NIBIB Biotechnology Resource Center.
37. R. Nachabé, D. J. Evers, B. H. W. Hendriks, G. W. Lucassen, M. van der Voort, J. Wesseling, T. J. M. Ruers, "Effect of bile absorption coefficients on the estimation of liver tissue optical properties and related implications in discriminating healthy and tumorous samples," *Biomed. Opt. Exp.* **2**, 600–614 (2011).
38. N. Rajaram, A. Gopal, X. Zhang, J. W. Tunnell. "Experimental validation of the effects of microvasculature pigment packaging on *in vivo* diffuse reflectance spectroscopy," *Lasers Surg. Med.* **42**(7), 680–688 (2010).
39. C. A. Schneider, W. S. Rasband, K. W. Eliceiri, "NIH Image to ImageJ: 25 years of image analysis," *Nat. Methods* **9**(7), 671–675 (2012).
40. Y. Fudaba, A. Oshita, H. Tashiro, H. Ohdan, "Intrahepatic triglyceride measurement and estimation of viability in rat fatty livers by near-infrared spectroscopy," *Hepatol. Res.* **45**(4), 470–479 (2015), doi: 10.1111/hepr.12364. Epub 2014 June 27.
41. D. G. Altman, J. M. Bland, "Absence of evidence is not evidence of absence," *Br. Med. J.* **311**(7003), 485 (1995).
42. F. Ge, H. Lobdell4th, S. Zhou, C. Hu, P. D. Berk, "Digital analysis of hepatic sections in mice accurately quantitates triglycerides and selected properties of lipid droplets," *Exp. Biol. Med. (Maywood)* **235**(11), 1282–1286 (2010), doi: 10.1258/ebm.2010.010095.
43. R. Veteläinen, A. van Vliet, T. M. van Gulik, "Essential pathogenic and metabolic differences in steatosis induced by choline or methione-choline deficient diets in a rat model," *J. Gastroenterol. Hepatol.* **22**(9), 1526–1533 (2007).
44. H. Marsman, T. Matsushita, R. Dierkhising, W. Kremers, C. Rosen, L. Burgart, S. L. Nyberg, "Assessment of donor liver steatosis: Pathologist or automated software?" *Hum. Pathol.* **35**(4), 430–435 (2004).
45. N. M. Gregg, B. R. White, B. W. Zeff, A. J. Berger, J. P. Culver, "Brain specificity of diffuse optical imaging: Improvements from superficial signal regression and tomography," *Front Neuroenerg.* **2**(pii), 14 (2010), doi: 10.3389/fnene.2010.00014.
46. S. H. Ibrahim, P. Hirsova, H. Malhi, G. J. Gores, "Animal models of nonalcoholic steatohepatitis: Eat, delete, and inflame," *Dig. Dis. Sci.* **61**(5), 1325–1336 (2016), doi: 10.1007/s10620-015-3977-1. Epub 2015 December 1.